Structural basis of light chain amyloidogenicity: Comparison of the thermodynamic properties, fibrillogenic potential and tertiary structural features of four Vλ6 proteins

ARTICLE *in* JOURNAL OF MOLECULAR RECOGNITION · JULY 2004

Impact Factor: 2.15 · DOI: 10.1002/jmr.681 · Source: PubMed

9 AUTHORS, INCLUDING:

Jonathan S Wall
The University of Tennessee Medical Center…
92 PUBLICATIONS **1,777** CITATIONS
SEE PROFILE

Vibha Gupta
Jaypee Institute of Information Technology
3 PUBLICATIONS **66** CITATIONS
SEE PROFILE

Remy Loris
Vrije Universiteit Brussel
150 PUBLICATIONS **4,156** CITATIONS
SEE PROFILE

Paul D Adams
Lawrence Berkeley National Laboratory
287 PUBLICATIONS **41,102** CITATIONS
SEE PROFILE

JOURNAL OF MOLECULAR RECOGNITION
J. Mol. Recognit. 2004; **17**: 323–331
DOI:10.1002/jmr.681

Structural basis of light chain amyloidogenicity: comparison of the thermodynamic properties, fibrillogenic potential and tertiary structural features of four $V_\lambda 6$ proteins

Jonathan S. Wall[1†], Vibha Gupta[2†], Matthew Wilkerson[2†], Maria Schell[1], Remy Loris[3], Paul Adams[4], Alan Solomon[1], Fred Stevens[5] and Chris Dealwis[2,6*]

[1]Human Immunology and Cancer Program, Department of Medicine, University of Tennessee Graduate School of Medicine, Knoxville, Tennessee, USA
[2]Department of Biochemistry, Cellular, and Molecular Biology, University of Tennessee, Knoxville, Tennessee, USA
[3]ULTR, Vrije Universiteit Brussels, Sintgenesius Rode, Belgium
[4]Structural Biology, Computational and Theoretical Biology, Lawrence Berkeley National Laboratory, Berkley, California, USA
[5]Biosciences Division, Argonne National Laboratory, Argonne, Illinois, USA
[6]Center for Excellence in Structural Biology, University of Tennessee, Knoxville, Tennessee, USA

Primary (AL) amyloidosis results from the pathologic deposition of monoclonal light chains as amyloid fibrils. Studies of recombinant-derived variable region (V_L) fragments of these proteins have shown an inverse relationship between thermodynamic stability and fibrillogenic potential. Further, ionic interactions within the V_L domain were predicted to influence the kinetics of light chain fibrillogenicity, as evidenced from our analyses of a relatively stable $V_\lambda 6$ protein (Jto) with a long range electrostatic interaction between Asp and Arg side chains at position 29 and 68, respectively, and an unstable, highly fibrillogenic $V_\lambda 6$ protein (Wil) that had neutral amino acids at these locations. To test this hypothesis, we have generated two Jto-related mutants designed to disrupt the interaction between Asp 29 and Arg 68 (JtoD29A and JtoR68S). Although the thermodynamic stabilities of unfolding for these two molecules were identical, they exhibited very different kinetics of fibril formation: the rate of JtoD29A fibrillogenesis was slow and comparable to the parent molecule, whereas that of JtoR68S was significantly faster. High-resolution X-ray diffraction analyses of crystals prepared from the two mutants having the same space group and unit cell dimensions revealed no significant main-chain conformational changes. However, several notable side-chain alterations were observed in JtoR68S, as compared with JtoD29A, that resulted in the solvent exposure of a greater hydrophobic surface and modifications in the electrostatic potential surface. We posit that these differences contributed to the enhanced fibrillogenic potential of the Arg 68 mutant, since both Jto mutants lacked the intrachain ionic interaction and were equivalently unstable. The information gleaned from our studies has provided insight into structural parameters that in addition to overall thermodynamic stability, contribute to the fibril forming propensity of immunoglobulin light chains.

Keywords: **X-ray diffraction; three-dimensional structure; amyloid; light chains; fibrillogenesis**

Received 26 February 2004; revised 16 March 2004; accepted 18 March 2004

INTRODUCTION

The aggregation of normally soluble proteins into fibrils and their deposition in vital tissues and organs are characteristic of a broad spectrum of diseases known as the amyloidoses (Falk *et al.*, 1997). There are more than 20 known amyloidogenic precursor proteins, e.g. β-peptide (Aβ), islet amyloid polypeptide (IAPP), α-synuclein, transthyretin (TTR) and immunoglobulin light chain proteins that are associated with Alzheimer's disease, type II diabetes, Parkinson's disease, familial polyneuropathy, and primary amyloidosis (AL), respectively (Sipe, 1994; Westermark *et al.*, 2002). Irrespective of the precursor protein, amyloid fibrils exhibit universal structural properties: they are 8–10 nm diameter fibers composed of bundled protofilaments and are of indeterminate length (Serpell *et al.*, 1999, 2000). The precursor proteins within the fibrillar array adopt a β-pleated sheet conformation with the strands oriented approximately perpendicular to the long axis of the fibril (Sunde and Blake, 1997). The characteristic nucleation-dependent kinetics of fibril formation *in vitro* and evidence for a critical protein concentration below which polymerization cannot occur liken fibrillogenesis to a crystallization process (Bishop and Ferrone, 1984; Harper and Lansbury, 1997; Serpell, 2000).

*Correspondence to: C. Dealwis, The University of Tennessee, Department of Biochemistry and Cellular and Molecular Biology, M407 Walters Life Sciences, Knoxville, TN 37996-0840, USA.
E-mail: cdealwis@utk.edu
†These authors made equal contributions to this work.
Contract/grant sponsor: National Cancer Institute and the Aslan Foundation; *contract/grant number:* CA10056.
Contract/grant sponsors: American Cancer Society; Physicians' Medical and Educational Research Foundation.

Abbreviations used: GdHCl, guanidine hydrochloride; LC, immunoglobulin light chain; V_L, immunoglobulin light chain variable domain.

```
          0          1          2          2          3          4
          1          1          1          8          5          5
λ6a       NFMLTQPHS* VSESPGKTVT ISCTRSSGS IASNYVQ WYQQRPGSSP TTVIYEDNQR
Wil         L                                N   H                  F  DH
Jto           N                            N  D              A  I
JtoD29A       N                            N  A              A  I
JtoR68S       N                            N  D              A  I

          5          6          7          8          9          9
          5          5   ab     3          3          3          9
λ6a       PSGVPDRFSG SIDSSSNSAS LTISGLKTED EADYYCQSYD SSN--- ----------
Wil                   V T                              HN QVF GGGTKLTVLG
Jto             A     R                                AR VVF GGGTRLTVLG
JtoD29A         A     R                                AR VVF GGGTRLTVLG
JtoR68S         A     S                                AR VVF GGGTRLTVLG
```

Figure 1. Comparison of the amino acid sequences of the $V_\lambda 6$ proteins Wil, Jto, JtoD29A, and JtoR68S with that of the predicted product of the λ6a germline gene.

Primary (AL) amyloidosis is characterized by the deposition in vital organs and tissues of fibrillar aggregates composed predominantly of the variable region (V_L) of monoclonal immunoglobulin light chains (LC). Clinically, patients with AL exhibit extreme morbidity which is usually fatal (Solomon and Weiss, 1995; Tan *et al.*, 1995; Rajkumar *et al.*, 1998; Bellotti *et al.*, 2000; Merlini and Bellotti, 2003). Comparative analyses have differentiated amyloid- from non-amyloid-associated proteins on the basis of certain amino acid substitutions at particular sites within the V_L (Raffen *et al.*, 1999; Stevens, 2000). Further, studies of the thermodynamic consequences of amino acid substitutions within these molecules have demonstrated an inverse correlation between protein stability and the propensity for fibril formation (Hurle *et al.*, 1994; Bellotti *et al.*, 1996; Raffen *et al.*, 1999; Wall *et al.*, 1999; Kim *et al.*, 2000, 2003). This relationship is also observed in other amyloidogenic precursor proteins, e.g. TTR (Hammarstrom *et al.*, 2002, 2003), prion protein (Safar *et al.*, 1993; Thual *et al.*, 2001) and lysozyme (Plaza del Pino *et al.*, 2000; Takano *et al.*, 2001).

In addition, the primary amino acid sequence has been shown to be predictive of fibril forming propensity (Chiti *et al.*, 2003). A thorough mutational analysis of human muscle acylphosphatase, a fibril-forming peptide not associated with amyloid disease, demonstrated a correlation between the fibrillogenic propensity of single amino acid mutants with three physical properties—hydrophobicity, charge and the propensity for α-helix to β-sheet transition (Chiti *et al.*, 2003). The rate of fibril elongation was linearly dependent upon these physicochemical properties (Chiti *et al.*, 1999, 2003).

Thermodynamic destabilization and the concomitant increase in fibril-forming propensity have been attributed, in LC proteins, to mutations that disrupt critical intrachain ionic interactions or remove proline residues that anchor the β-sheet network, as well as those that introduce glycosylation sites (Omtvedt *et al.*, 2000; Stevens, 2000). As a result of destabilization the V_L domain can adopt non-native structural conformations that may be pro-amyloidogenic, thus facilitating the formation of fibrils (Khurana *et al.*, 2001, 2003a, b; Kim *et al.*, 2003). The precise structural and physicochemical penalties for destabilizing the light chain V_L domain that lead to enhanced fibrillogenicity remain enigmatic. However, decreases in the thermodynamic stability of amyloidogenic proteins can result in: dissociation of stable oligomeric complexes (McCutchen *et al.*, 1993; Jiang *et al.*, 2001); increased hydrophobicity indicated by the enhanced fluorescence emission of the dye ANS (Souillac *et al.*, 2002, 2003; Khurana *et al.*, 2003b); compaction of the protein, evidenced by a decrease in the radius of gyration (Souillac *et al.*, 2003); and, the dislocation of loops in the polypeptide chain from the body of the protein, thereby exposing novel interfaces that may support self-association (Davis *et al.*, 2000).

Monoclonal light chains of the $V_\lambda 6$ subgroup are, with one notable exception, invariably associated with primary (AL) amyloidosis. We have shown that a comparison of two $V_\lambda 6$ proteins, Jto and Wil, the former derived from a patient with multiple myeloma who had no clinical manifestation of amyloidosis and the latter obtained from an amyloidotic individual, revealed differences in the thermodynamic stability of unfolding that correlated with the rates of fibril formation *in vitro* (Wall *et al.*, 1999). Based on X-ray diffraction data on crystals prepared from these two molecules, we posited that the increased stability of protein Jto resulted from a unique ionic surface interaction between residues Asp29 and Arg68 that was not present in the unstable fibrillogenic protein Wil due to the presence of uncharged amino acids at these two positions (Pokkuluri *et al.*, 1999). To test this hypothesis, we have generated two mutant Jto variants, designated JtoD29A and JtoR68S, in which the residues at position 29 and 68 were replaced by their germline-encoded counterparts, Ala and Ser, respectively (Fig. 1). We now report the results of our comparative studies of the thermodynamic stability, kinetics of fibrillogenesis, and tertiary structural features of these two mutants with those of native Jto and the amyloidogenic protein Wil. These analyses have demonstrated that in addition to the overall thermodynamic stability of the V_L domain, hydrophobic and electrostatic perturbations arising from the mutations can influence light chain amyloid formation.

EXPERIMENTAL PROCEDURE

Protein expression and purification

The cDNA encoding the $V_\lambda 6$ Jto protein was prepared from an enriched population of monoclonal plasma cells isolated from the bone marrow of patient Jto and sub-cloned into a pET-27(+) vector for protein expression in *E. coli*. The procedures for cloning, protein expression, and purification

of the $V_\lambda 6$ Jto proteins have been previously described (Wall *et al.*, 1999). The JtoD29A and JtoR68S mutations were constructed using Stratagene Quick-Change site-directed mutagenesis kit. Oligonucleotides containing the appropriate base changes, D29A and R68S, were used to amplify by PCR the $V_\lambda 6$Jto/pET-27 plasmid. The template product was digested with the Dpn1 nuclease and the daughter plasmids transformed into DH5α *E. coli*. The mutant $V_\lambda 6$ proteins JtoD29A and JtoR68S were re-transformed for protein production in *E. coli* (Wall *et al.*, 1999).

Thermodynamic and fibrillogenesis analyses

The folding stabilities of the purified JtoD29A and JtoR68S proteins were determined by incubation in solutions of increasing molar concentrations of guanidine hydrochloride (GdHCl), as previously described. The values of C_m and ΔG_{H_2O}, represent, respectively, the concentration of GdHCl required to achieve 50% unfolding in a two-state transition and the free energy of stabilization extrapolated to pure water. Fibrillogenesis kinetics were monitored at 37 °C using a solution containing 3 μM protein, 10 μM thioflavin T, 150 mM sodium chloride, and 10 mM phosphate buffer, pH 7.5. An increase in the fluorescence intensity of the thioflavin T measured at 490 nm (excitation, 450 nm) was indicative of fibril formation (Naiki *et al.*, 1989; Wall *et al.*, 1999). Aggregates formed in the reactions were confirmed as fibrils by negative-stain electron microscopic analyses, as previously described (Wall *et al.*, 1999).

Crystallization conditions

Crystals were grown by vapor diffusion at room temperature. JtoD29A was crystallized in a mother liquor of 0.8 M ammonium sulfate, 0.1 M sodium acetate, pH 5.0, and containing 0.1 M cadmium chloride. A 10 mg/ml solution of JtoD29A protein was equilibrated with the mother liquor at a ratio of 1:1. The crystals were improved by additions of the detergent *n*-decyl-B-D-maltoside added to the hanging drop at its CMC. JtoR68S was crystallized under similar conditions except higher concentrations of cadmium chloride (40 mM) and protein (14 mg/ml) were used in the mother liquor.

Data collection and reduction

JtoD29A and JtoR68S crystals were cryoprotected by soaking in their respective mother liquors containing 10–15% glycerol. Diffraction data for JtoR68S and JtoD29A were collected at a temperature of −160 °C and a wavelength of 1.5418 Å on a Rigaku RU-H3R rotating anode X-ray generator with osmic focusing mirrors using a R-axis IV^{++} image plate detector to 1.9 and 2.5 Å, respectively. High-resolution data on JtoD29A crystals were collected at −160 °C and a wavelength of 0.97622 Å using a Mar image plate detector at the synchrotron instrument in Hamburg on a DESY 9 source at the BW7A beamline. The data were indexed, integrated, and scaled using the programs DENZO and SCALEPACK (Minor *et al.*, 2000). The SCALEPACK data were converted to the mtz format using the CCP4 program SCALEPACK2MTZ, and the structure factors were calculated using the program TRUNCATE that implements French and Wilson statistics (French and Wilson, 1978). In order to determine the space group, pseudo precession pictures using the CCP4 script HKLVIEW were created.

Structure determination

The JtoD29A and JtoR68S structures were solved using the molecular replacement method (Brick and Blow, 1987), with the program AMoRe (Navaza, 1994) implemented in the crystallographic suite CCP4 (Collaborative Computational Project 1994). In AMoRe, ROTING calculates the rotation function, TRAING calculates the translation function, and FITTING performs a rigid-body refinement of the structure. The starting model used for JtoD29A and JtoR68S was the $V_\lambda 6$ Jto dimer (PDB no. 1CD0), which crystallized in the space group $P2_12_12_1$, with $a = 68.018$ Å, $b = 58.388$ Å, $c = 59.037$ Å, $\alpha = \beta = \gamma = 90°$. Data in the resolution range of 50–3.0 Å were used for conducting molecular replacement and the radius of integration was 0.0–23.738 Å. PDB accession codes were 1PEW for JtoD29A and 1PW3 for JtoR68S. For JtoR68S, the correlation coefficients from the translation function were 25.0 and 24.7%, respectively, for the two molecules/asymmetric unit. The largest noise peak had a correlation coefficient of 13%. After fixing molecule one to find the relative position of the second molecule using TRAING, the correlation coefficient increased to 40.4%. Final fitting using the program FITTING further increased the correlation coefficient to 67.2%. For JtoD29A, the correlation coefficients from the translation function were 23.1 and 20.2%, respectively, for the two molecules/asymmetric unit. After fixing molecule 1 to find the relative position of the second molecule, the correlation coefficient increased to 39.4%. Final fitting improved the correlation coefficient to 65.6%.

To fine tune the three orientation and three translational parameters the original solutions from MR were subjected to rigid-body refinement with CNS (Brünger *et al.*, 1998). This was followed by a round of simulated annealing and positional refinement, using the amplitude-based maximum likelihood target (MLF) in CNS. After glycine was substituted at the position of the mutations, $2F_o–F_c$ difference Fourier maps were calculated and displayed using the graphics program O (Jones *et al.*, 1991). At this stage the replacements of Ser68 in JtoR68S and Ala29 in JtoD29A were conducted with the graphics program O. After several alternating rounds of positional refinement and model building with CNS and O, the refinement procedure was continued using the maximum likelihood method-based REFMAC (Murshudov *et al.*, 1996) in the CCP4 suite. Finally, both structures were subjected to B-factor refinement using REFMAC.

Both proteins crystallized in the space group $P4_122$ (Table 1). The final model of JtoD29A was refined to a crystallographic *R* value (R_{cryst}) of 25.2% and an R_{free} value of 27% (R_{free} was calculated with 5% of the data) at 2.0 Å resolution. The rms deviations from ideality in bond angles and bond lengths were 1.219° and 0.017 Å, respectively. For

Table 1. Data collection and refinement statistics

	JtoD29A	JtoR68S
Number of molecules per asymmetric unit	2	2
R_{sym}	6.5%	6.6%
Resolution	14.74–2	15.00–1.90
Completion	99.5%	95%
R_{cryst}	25.2%	21.5%
R_{free}	27.0%	23.3%
Non-hydrogen protein atoms/asymmetric unit	1766	1820
Metal ions/asymmetric unit	4	4
Water molecules/ asymmetric unit	107	115
rms Deviations from ideality		
Bond lengths (Å)	0.017	0.009
Bond angles (deg)	1.219	1.19
Space group	P 4(1)22	P 4(1)22
Unit cell dimensions	73.6 Å × 73.6 Å × 92.3 Å 90°, 90°, 90°	72.2 Å × 72.2 Å × 94.3 Å 90°, 90°, 90°

JtoR68S the final model was refined to a crystallographic *R*-value (R_{cryst}) of 21.5% and an R_{free} value of 23.34% at 1.9 Å resolution. The rms deviations from ideality in bond angles and bond lengths were 1.19° and 0.009 Å, respectively.

The average main and side-chain B-factors for the JtoR68S molecule were 16.3 and 18.3 $Å^2$, respectively. The corresponding *B*-factors for JtoD29A were 22.8 and 25.9 $Å^2$, respectively. The fact that the rms difference between molecules A and B of both the JtoD29A and JtoR68S crystals (0.438 and 0.516 Å, respectively) were minimal indicated that both forms were essentially identical. Therefore, structural comparisons of the two Jto variants were performed with molecule A alone.

RESULTS AND DISCUSSION

Thermodynamic stability

The unfolding curves of the four $V_\lambda 6$ proteins Jto, JtoD298, JtoR68S and Wil, as determined in the presence of increasing concentrations of GdHCl, revealed midpoints (C_ms) of 1.22 M (ΔG_{H_2O}, 4.3 kcal/mol), 1 M (ΔG_{H_2O}, 3.2 kcal/mol), 1 M (ΔG_{H_2O}, 3.2 kcal/mol), and 0.83 M (ΔG_{H_2O}, 2.2 kcal/mol), respectively [Fig. 1(A)]. The 1.1 kcal/mol decrease in ΔG_{H_2O} for the two Jto mutants represented ~25% of the total net folding stability. In Jto mutants the degree of destabilization was approximately the same when either Asp29 or Arg68 was replaced by the uncharged germline residue.

The lag times and rates of fibril formation of protein Jto and Wil correlated with their thermodynamic stabilities (Wall *et al.*, 1999). Owing to their decreased stability, it was anticipated that both JtoD29A and JtoR68S single mutant variants would exhibit properties intermediate to those in the native and Jto and Wil proteins, for example they should exhibit equivalently shorter lag times in fibrillogenesis kinetics with respect to native Jto. Experimentally, the JtoR68S protein showed a lag time 5-fold faster (~7000 s) than that of Jto, but this was still slower than that of protein Wil, a result consistent with its intermediate folding stability. Surprisingly, the JtoD29A variant had a lag time equivalent to that of the native Jto molecule [Fig. 2(B)]. The formation of fibrils by both Jto variants was confirmed by electron microscopy [Fig. 2(C, D)]. Within experimental

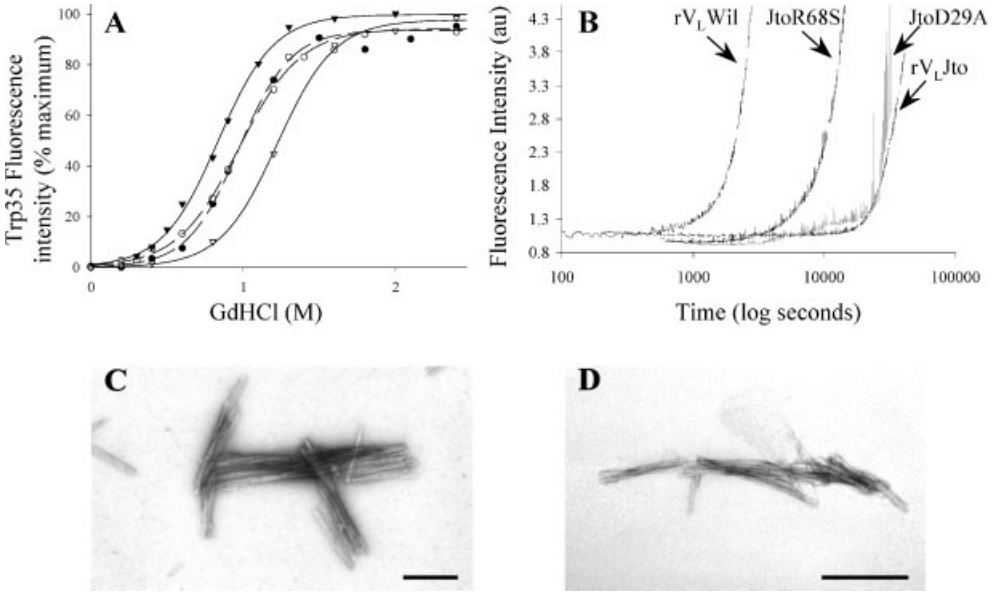

Figure 2. Stability and Fibrillogenesis of $V_\lambda 6$ proteins: (A) thermal unfolding experiments established the relative stabilities of $V_\lambda 6$Wil, $V_\lambda 6$Jto, JtoD29A, and JtoR68S—(▼) $V_\lambda 6$Wil; (○) JtoD29A; (●) JtoR68S; (▽) $V_\lambda 6$Jto. (B) Kinetics of $V_\lambda 6$ protein fibril formation at 37 °C monitored by changes in the fluorescence intensity of thioflavin T. Electron microscopic analysis of fibrils formed by JtoR68S (C) and JtoD29A (D); the bar in both figures is 200 nm.

error the JtoD29A and JtoR68S mutants had almost superimposable chaotropic denaturation curves; however, the latter molecule exhibited a 5-fold shorter lag time in the kinetics of fibril formation. Thus, the kinetics of fibril formation of the two $V_\lambda 6$ variants could not be explained simply in terms of their ΔG values of unfolding. We therefore examined the three-dimensional structures of Jto, Wil and the Jto mutants for additional insight into this anomalous observation.

X-ray analyses of JtoD29A and JtoR68S

After glycine was substituted at the site of the two mutations, the $2F_o–F_c$ omit maps derived after several rounds of first rigid-body refinement and positional refinement unambiguously defined the electron density of the mutated residues in both JtoD29A and JtoR68S [Fig. 3(A) and (B)]. Both JtoD29A and JtoR68S were crystallized in the presence of cadmium chloride. Four bound Cd^{2+} ions per asymmetric unit were identified in each protein; and 107 and 115 water molecules were included in the final refinements of JtoD29A and JtoR68S, respectively. In the former, residues 39–42 were disordered.

To determine whether significant main-chain conformational changes accompanied the substitutions of residues at position 29 and 68, the structures of JtoD29A and JtoR68S were superimposed with those of the stable (native) Jto and unstable Wil $V_\lambda 6$ proteins [Fig. 3(C)]. All four molecules were virtually identical except for regions within the immediate vicinity of the Asp29Ala and Arg68Ser mutations. The Cα main-chain rms differences between Jto and the JtoD29A, JtoR68S and Wil proteins were 1.368, 0.669, and 0.865 Å, respectively. Given the $>90\%$ sequence identity among these $V_\lambda 6$ molecules (Fig. 1), the Cα rms values reflected the high degree of primary structural homology. Although the main-chain conformations were almost identical, several notable side-chain conformational differences were found at the site of the mutations. Loss of Arg68 facilitated the formation of a new hydrogen bond between the carboxyl oxygen of Asp29 and the ND1 atom of Asn31 [Fig. 3(D)]. The hydroxyl group of the substituted Ser68 in the same mutant was solvent exposed and not involved in hydrogen bonding interactions with other parts of the protein. In JtoD29A, substitution of Asp29 allowed the guanidinium group of Arg68 to turn toward the solvent [Fig. 3(D)]. In contrast to the JtoR68S variant, the side-chain conformation of Asn31 in the JtoD29A mutant was identical to that of the native Jto structure.

Because JtoD29A and JtoR68S crystallized in the same space group with nearly identical unit cell dimensions, it was possible to perform detailed comparisons of the hydrophobic surface accessible and electrostatic potential surface areas.

Hydrophobic effects

There was a 42.5 $Å^2$ increase in solvent accessibility of hydrophobic residues (Gly, Ala, Val, Ile, Leu, Met and Phe) in JtoR68S as compared with JtoD29A, indicating that loss of Arg69 propagated the exposure of a larger hydrophobic surface area with respect to the D29A substitution. We also investigated whether there were differences in the solvent exposure of apolar atoms in all side-chains in the two $V_\lambda 6$ Jto variants. Residues at 14 positions were shown to have higher apolar surface accessibilities in JtoR68S as compared to JtoD29A (Fig. 4). Interestingly, the affected residues were not randomly positioned around the domain; rather they were clustered into two regions: one located between residues 5 and 32 and the second between positions 61–79 (Fig. 4). These observations were consistent with findings from a difference distance matrix plot analysis of JtoR68S vs JtoD29A (data not shown). The first cluster, which lay within the first β-hairpin loop, contained a majority of the exposed apolar atoms. The second consisted of a strand adjacent to the relatively apolar N-terminal β-hairpin loop (Fig. 4). The β-strand between residues 70 and 80 of the $V_\kappa 4$ protein Len is complementary to the binding site of the light chain chaperone protein BiP (Davis *et al.*, 2000; Dul *et al.*, 2001). It is possible that this region becomes displaced, revealing novel interfaces that may be involved in fibril formation. Indeed, a synthetic peptide mimicking residues 74–80 of the $\kappa 4$ protein Len inhibited the fibrillogenesis of the Len V_L protein *in vitro*, indicating the importance of this region in self-association during fibril-formation (Davis *et al.*, 2000).

Electrostatic effects

We compared the electrostatic potential surfaces of the two $V_\lambda 6$ Jto mutants using the program Delphi. The native Jto had a net charge of -2, as compared to values of -1 and -3 in JtoD29A and JtoR68S, respectively. The effects of the mutations and the accompanying changes in net charge were readily apparent on the electrostatic potential surface maps (Fig. 5). The electrostatic potential surface of JtoR68S appeared to exhibit a well-defined dipole, as compared with Jto and JtoD29A (Fig. 5). JtoD29A exhibited a localized increase in positive electrostatic potential away from the site of the mutation. We attributed this increase to the movement of the guanidinium side-chain of Arg54, indicating that the loss of Asp29 has had long-range effects on protein structure and perhaps function (Fig. 5).

Although exhibiting equivalent folding stabilities, the less fibrillogenic JtoD29S variant was characterized by a more hydrophilic surface area surface area and a difference of $+2$ in the net charge with respect to the fibrillogenic JtoR68S mutant. Chiti *et al.* have shown that mutations that increase the hydrophobicity or increase the net negative charge of proteins or peptides render them more fibrillogenic (Chiti *et al.*, 2003). This correlation was determined by measuring the formation of fibrils from unstructured peptides and unfolded proteins, not from the native state ensemble. Our data do not conform to this analysis because the fibrillogenesis of Jto mutants was measured under conditions where the native state ensemble was highly populated. The contention presented here is that the mutation in JtoR68S led to decreased stability and physicochemical modifications that favor fibrillogenesis. In JtoD29A thermodynamic stability was also decreased, but the substitution did not affect the resistance to form fibrils. Mutations in TTR have been found to enhance fibrillogenicity, not by decreasing the equilibrium thermodynamic stability

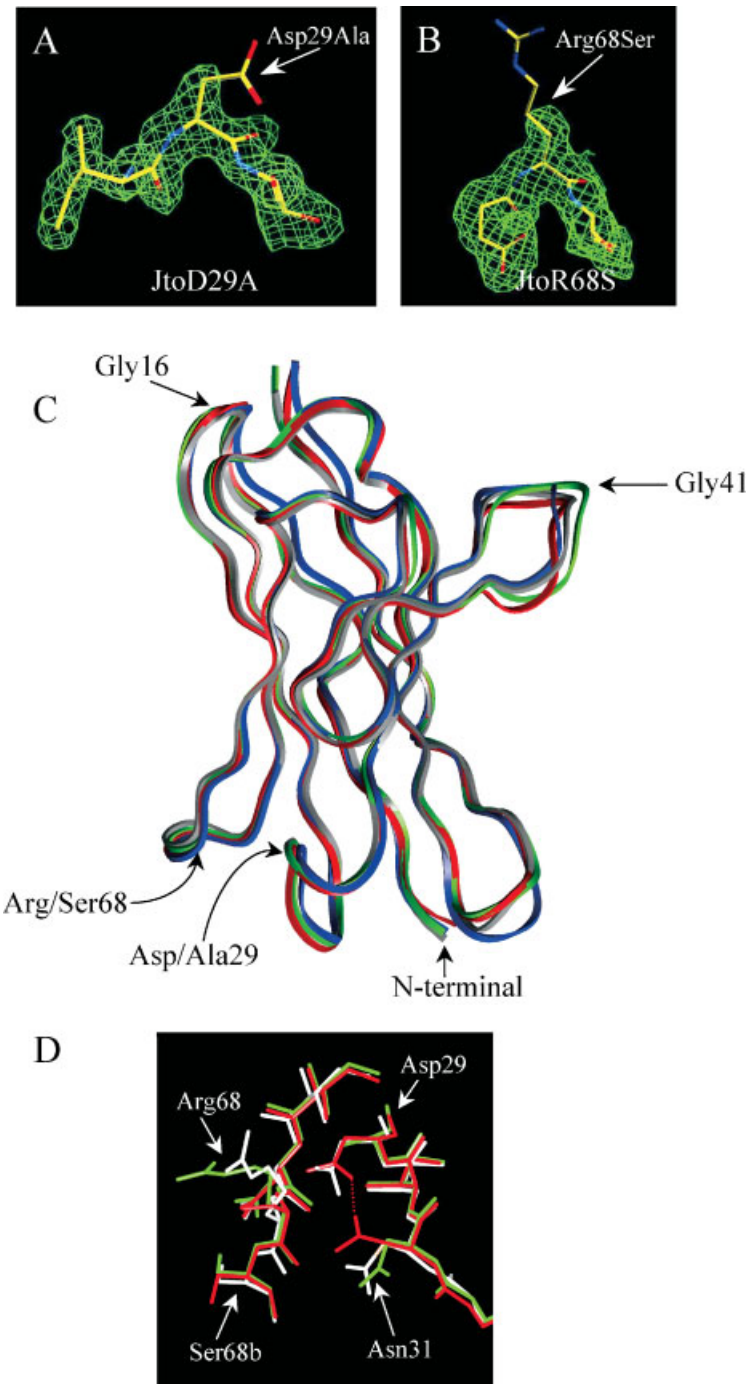

Figure 3. Structural comparison of V_λ6Jto mutants. $2F_o$–F_c omit maps generated at the site of the mutation for (A) JtoD29A and (B) JtoR68S (contour level, 1 σ). (C) Main-chain Cα superposition of V_λ6Jto (gray), JtoD29A (green), JtoR68S (red), and V_λ6Wil (blue). (D) Superposition of V_λ6Jto (white), JtoD29A (green), and JtoR68S (red) around the sites of this mutated residues at positions 29 and 68. A new hydrogen bond formed between Asp29 and Asn31 is represented by the red dotted line (prepared using the Insight II program).

but by increasing the dissociation rate of the stable tetramer—a prerequisite for fibril formation (Jiang *et al.*, 2001).

Our studies of the thermodynamic properties, fibrillogenic potential, and tertiary structure of four homologous V_λ6 molecules have provided evidence that factors other than thermodynamic stability influence the amyloidogenic propensities of immunoglobulin light chain V_L domains. The data contradicted the expected correlation between increased fibrillogenic propensity and decreasing folding stability in an unexpected, yet not unique fashion. Previously, we had shown that the destabilization of a non-amyloidogenic κ1 LC (GAL), to a level equivalent to that of the amyloidogenic BIF κ1 domain, led to formation of soluble aggregates, but not to discrete fibrils (Kim *et al.*,

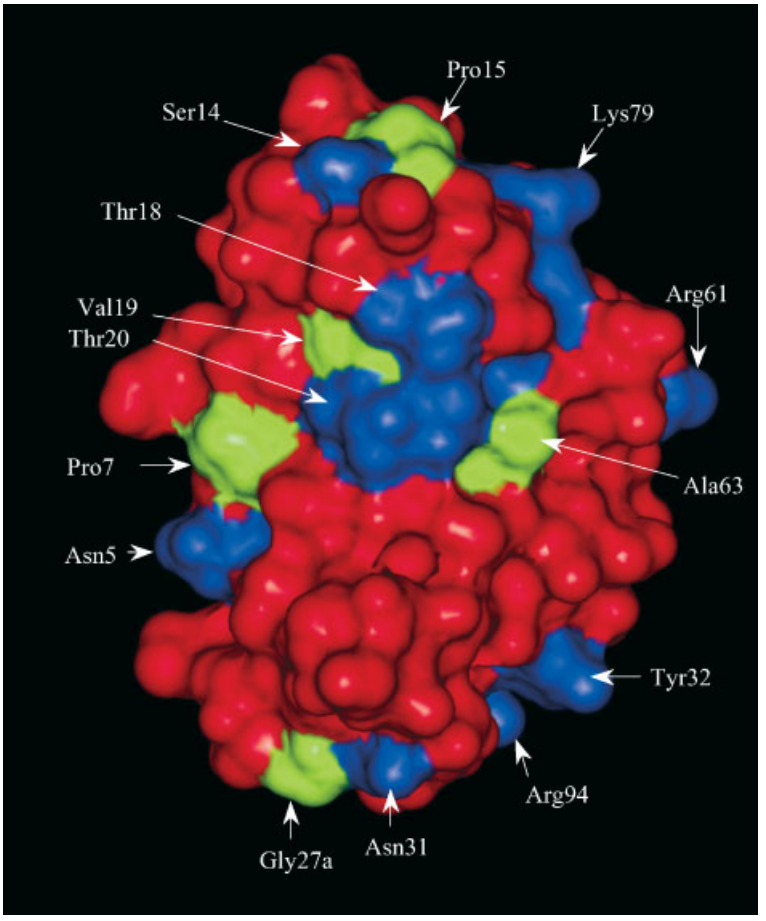

Figure 4. Comparison of accessible apolar surface area in JtoD29A and JtoR68S. The surface area was calculated for JtoD29A, and JtoR68S using the program ACCESS. The hydrophobic residues are shown in green and the blue residues denote apolar regions. The figure was prepared using the Insight II program.

2000). The finding that the kinetics of fibril formation by mutant Jto proteins (particularly JtoD29A) could not be attributed solely to folding stability suggested that other factors were involved. A similar discordance has been noted between the stability of certain human cellular prion protein mutants and the observed disease phenotype (Liemann and Glockshuber, 1999).

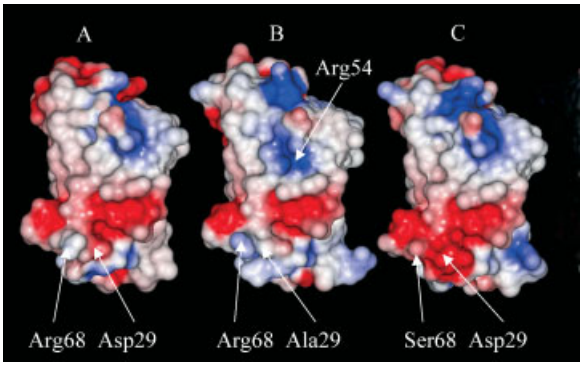

Figure 5. Comparison of the electrostatic potential surfaces of (A) $V_{\lambda}6$Jto, (B) JtoD29A and (C) JtoR68S. The neutral, positive and negatively charged residues appear white, blue and red, respectively (prepared using the Insight II program).

Comparative analysis of the tertiary structural features of the four $\lambda 6\ V_L$ domains of varying fibrillogenic potential indicated subtle physicochemical differences between Jto and its mutants. These differences were manifest in the area of exposed hydrophobic surface area and in negative electrostatic potential surface area. Further analysis of the impact of each mutation on the thermodynamic stability and fibrillogenic propensity has provided a model to rationalize the data.

Taken as a pair, the combined contribution of Asp29 and Arg68 to the overall stability of the V_L domain in Jto was calculated to be approximately 2 kcal/mol compared with the stability of Wil, with neutral germline-like residues at these positions (ΔGJto $- \Delta G$Wil $= 2.1$ kcal/mol). When calculated separately, the difference in stability (ΔGJto $- \Delta G$Jto$_{mutant}$) was found to be 1.1 kcal/mol for each of the substitutions of Asp29 for Ala or Arg68 for Ser. Thus, the two replacements were energetically similar. Together, they equaled the double mutant in contributing to the stability of the Jto V_L domain. Further calculations suggested that the coupling free energy of the Asp29:Arg68 long-range electrostatic interaction was negligible and relatively unimportant (Bosshard *et al.*, 2004). Therefore, the increased domain stability associated with the Asp29 and Arg68 substitutions may be attributed to the increased

hydrophilicity of these residues with respect to their germline encoded counterparts—Ala and Ser, respectively. The relative hydrophilicity values are 3.0 for aspartic acid, 3.0 for arginine, but only −0.5 for alanine and 0.3 for serine (Hopp, 1989).

Considering the appearances of Asp29 and Arg68 independently, we next assessed the impact of each mutation on the fibrillogenic potential of the highly amyloidogenic λ6 polypeptide sequence. Clinical observations previously demonstrated recurring correlations between products of the λ6 germline gene and amyloid disease (Ozaki *et al.*, 1994). The Asp29:Ser68 pairing in JtoR68S yielded a highly fibrillogenic variant with reaction kinetics similar to those of protein Wil. The Ala29:Arg68 variant (JtoD29A), however, exhibited significantly slower fibril formation, equivalent to that of protein Jto. Thus, the presence of Arg68 alone was sufficient to slow the rate of fibril formation. It is interesting that Arg68 immediately precedes the two-residue insertion (68a and b in framework 3) that is unique to the λ6 subgroup. This region has been targeted as a probable participant in the formation of fibrils. A bulky, fully charged and highly solvated Arg side chain in this region may sterically, electrostatically or entropically interfere with what is an otherwise highly efficient polymerization process.

Acknowledgements

We are thankful to Brad Bennett and James Goodin for their critical review of this manuscript and Professor Allen Edmundson for his excellent discussions and insight. We appreciate the assistance of Dr. John Dunlap (University of Tennessee, Knoxville, TN, USA) in performing the electron microscopic analyses. We acknowledge Drs Elias Fernandez, Elias Lolis, Steven Sprang, Willia Lipscomb and Greg Petsko for useful discussion.

REFERENCES

Bellotti V, Stoppini M, Mangione PP, Fornasieri A, Min L, Merlini G, Ferri G. 1996. Structural and functional characterization of three human immunoglobulin kappa light chains with different pathological implications. *Biochim. Biophys. Acta* **1317**(3): 161–167.

Bellotti V, Mangione P, Merlini G. 2000. Review: immunoglobulin light chain amyloidosis—the archetype of structural and pathogenic variability. *J. Struct. Biol.* **130**: 280–289.

Bishop MF, Ferrone FA. 1984. Kinetics of nucleation-controlled polymerization. A perturbation treatment for use with a secondary pathway. *Biophys. J.* **46**: 631–644.

Bosshard HR, Marti DN, Jelesarov I. 2004. Protein stabilization by salt bridges: concepts, experimental approaches and clarification of some misunderstandings. *J. Mol. Recognit.* **17**(1): 1–16.

Brick P, Blow DM. 1987. Crystal structure of a deletion mutant of a tyrosyl-tRNA synthetase complexed with tyrosine. *J. Mol. Biol.* **194**(2): 287–297.

Brünger AT, Adams P, Clore G, Delano W, Gros P, Grosse-Kuntsleve R, Jiang J, Kuszewski J, Nilges M, Pannu N, Read R, Rice L, Simonson T, Warren G. 1998. Crystallography and NMR System: a new software suite for macromolecular structure determination. *Acta Crystallogr. D* **54**: 905–921.

Chiti F, Webster P, Taddei N, Clark A, Stefani M, Ramponi G, Dobson CM. 1999. Designing conditions for in vitro formation of amyloid protofilaments and fibrils. *Proc. Natl Acad. Sci. USA* **96**(7): 3590–3594.

Chiti F, Stefani M, Taddei N, Ramponi G, Dobson CM. 2003. Rationalization of the effects of mutations on peptide and protein aggregation rates. *Nature* **424**(6950): 805–808.

Collaborative Computational Project N. 1994. The CCP4 suite: programs for protein crystallography. *Acta Crystallogr. D* **50**: 760–763.

Davis PD, Raffen R, Dul LJ, Vogen MS, Williamson KE, Stevens JF, Argon Y. 2000. Inhibition of amyloid fiber assembly by both BiP and its target peptide. *Immunity* **13**(4): 433–442.

Dul JL, Davis DP, Williamson EK, Stevens FJ, Argon Y. 2001. Hsp70 and antifibrillogenic peptides promote degradation and inhibit intracellular aggregation of amyloidogenic light chains. *J. Cell. Biol.* **152**(4): 705–716.

Falk RH, Comenzo RL, Skinner M. 1997. The systemic amyloidoses. *New Engl. J. Med.* **337**(13): 898–909.

French S, Wilson K. 1978. On the treatment of negative intensities. *Acta Crystallogr. A* **34**: 517–525.

Hammarstrom P, Jiang X, Hurshman AR, Powers ET, Kelly JW. 2002. Sequence-dependent denaturation energetics: a major determinant in amyloid disease diversity. *Proc. Natl Acad. Sci. USA* **99**(Suppl. 4): 16427–16432.

Hammarstrom P, Wiseman RL, Powers ET, Kelly JW. 2003. Prevention of transthyretin amyloid disease by changing protein misfolding energetics. *Science* **299**(5607): 713–716.

Harper JD, Lansbury PT. 1997. Models of amyloid seeding in Alzheimer's disease and scrapie: mechanistic truths and physiological consequences of the time-dependent solubility of amyloid proteins. *A. Rev. Biochem.* **66**: 385–407.

Hopp TP. 1989. Use of hydrophilicity plotting procedures to identify protein antigenic segments and other interaction sites. *Meth. Enzymol.* **178**: 571–585.

Hurle MR, Helms LR, Li L, Chan W, Wetzel R. 1994. A role for destabilizing amino acid replacements in light-chain amyloidosis. *Proc. Natl Acad. Sci. USA* **91**(12): 5446–5450.

Jiang X, Buxbaum JN, Kelly JW. 2001. The V122I cardiomyopathy variant of transthyretin increases the velocity of rate-limiting tetramer dissociation, resulting in accelerated amyloidosis. *Proc. Natl Acad. Sci. USA* **98**(26): 14943–14948.

Jones TA, Zou JY, Cowan SW, Kjeldgaard M. 1991. Improved Methods for binding protein models in electron density maps and the location of errors in these models. *Acta Crystallogr. A* **47**: 110–119.

Khurana R, Gillespie JR, Talapatra A, Minert LJ, Ionescu-Zanetti C, Millett I, Fink AL. 2001. Partially folded intermediates as critical precursors of light chain amyloid fibrils and amorphous aggregates. *Biochemistry* **40**(12): 3525–3535.

Khurana R, Ionescu-Zanetti C, Pope M, Li J, Nielson L, Ramirez-Alvarado M, Regan L, Fink AL, Carter SA. 2003a. A general model for amyloid fibril assembly based on morphological studies using atomic force microscopy. *Biophys. J.* **85**(2): 1135–1144.

Khurana R, Souillac PO, Coats AC, Minert L, Ionescu-Zanetti C, Carter SA, Solomon A, Fink AL. 2003b. A model for amyloid fibril formation in immunoglobulin light chains based on comparison of amyloidogenic and benign proteins and specific antibody binding. *Amyloid* **10**(2): 97–109.

Kim Y, Wall JS, Meyer J, Murphy C, Randolph TW, Manning MC, Solomon A, Carpenter JF. 2000. Thermodynamic modulation of light chain amyloid fibril formation. *J. Biol. Chem.* **275**(3): 1570–1574.

Kim YS, Randolph TW, Manning MC, Stevens FJ, Carpenter JF. 2003. Congo red populates partially unfolded states of an

amyloidogenic protein to enhance aggregation and amyloid fibril formation. *J. Biol. Chem.* **278**(12): 10842–10850.
Liemann S, Glockshuber R. 1999. Influence of amino acid substitutions related to inherited human prion diseases on the thermodynamic stability of the cellular prion protein. *Biochemistry* **38**(11): 3258–3267.
McCutchen SL, Colon W, Kelly JW. 1993. Transthyretin mutation Leu-55-Pro significantly alters tetramer stability and increases amyloidogenicity. *Biochemistry* **32**(45): 12119–12127.
Merlini G, Bellotti V. 2003. Molecular mechanisms of amyloidosis. *New Engl. J. Med.* **349**(6): 583–596.
Minor W, Tomchick D, Otwinowski Z. 2000. Strategies for macromolecular synchrotron crystallography. *Structure Fold Des.* 15;**8**(5): R105–R110.
Murshudov G, Vagin E, Dobson E. 1996. Application of maximum likelihood refinement. *The Refinement of Protein structures, Proceedings of Daresbury Study Weekend*.
Naiki H, Higuchi K, Hosokawa M, Takeda T. 1989. Fluorometric determination of amyloid fibrils *in vitro* using the fluorescent dye, thioflavin T1. *Anal. Biochem.* **177**(2): 244–249.
Navaza J. 1994. AMoRe: an automated package for molecular replacement. *Acta Crystallogr. A.* **50**: 157–163.
Omtvedt LA, Bailey D, Renouf DV, Davies MJ, Paramonov NA, Haavik S, Husby G, Sletten K, Hounsell EF. 2000. Glycosylation of immunoglobulin light chains associated with amyloidosis. *Amyloid* **7**(4): 227–244.
Ozaki S, Abe M, Wolfenbarger D, Weiss DT, Solomon A. 1994. Preferential expression of human l-light-chain variable-region subgroups in multiple myeloma, AL amyloidosis, and Waldenstroms macroglobulinemia. *Clin. Immunol. Immunopatho.* **71**: 183–189.
Plaza del Pino IM, Ibarra-Molero B, Sanchez-Ruiz JM. 2000. Lower kinetic limit to protein thermal stability: a proposal regarding protein stability *in vivo* and its relation with misfolding diseases. *Proteins* **40**(1): 58–70.
Pokkuluri PR, Solomon A, Weiss DT, Stevens FJ, Schiffer M. 1999. Tertiary structure of human lambda 6 light chains. *Amyloid* **6**(3): 165–171.
Raffen R, Dieckman LJ, Szpunar M, Wunschl C, Pokkuluri PR, Dave P, Wilkins Stevens P, Cai X, Schiffer M, Stevens FJ. 1999. Physicochemical consequences of amino acid variations that contribute to fibril formation by immunoglobulin light chains. *Protein Sci.* **8**(3): 509–517.
Rajkumar SV, Gertz MA, Kyle RA. 1998. Prognosis of patients with primary systemic amyloidosis who present with dominant neuropathy. *Am. J. Med.* **104**(3): 232–237.
Safar J, Roller PP, Gajdusek DC, Gibbs CJ Jr. 1993. Thermal stability and conformational transitions of scrapie amyloid (prion) protein correlate with infectivity. *Protein Sci.* **2**(12): 2206–2216.
Serpell LC. 2000. Alzheimer's amyloid fibrils: structure and assembly. *Biochim. Biophys. Acta* **1502**(1): 16–30.
Serpell LC, Fraser PE, Sunde M. 1999. X-ray fiber diffraction of amyloid fibrils. *Meth. Enzymol.* **309**: 526–536.
Serpell LC, Sunde M, Benson MD, Tennent GA, Pepys MB, Fraser PE. 2000. The protofilament substructure of amyloid fibrils. *J. Mol. Biol.* **300**(5): 1033–1039.
Sipe JD. 1994. Amyloidosis. *Crit. Rev. Clin. Lab. Sci.* **31**(4): 325–354.
Solomon A, Weiss DT. 1995. Protein and host factors implicated in the pathogenesis of light chain amyloidosis (AL amyloidosis). *Amyloid: Int. J. Exp. Clin. Invest.* **2**: 269–279.
Souillac PO, Uversky VN, Millett IS, Khurana R, Doniach S, Fink AL. 2002. Elucidation of the molecular mechanism during the early events in immunoglobulin light chain amyloid fibrillation. Evidence for an off-pathway oligomer at acidic pH. *J. Biol. Chem.* **277**(15): 12666–12679.
Souillac PO, Uversky VN, Fink AL. 2003. Structural transformations of oligomeric intermediates in the fibrillation of the immunoglobulin light chain LEN. *Biochemistry* **42**(26): 8094–8104.
Stevens FJ. 2000. Four structural risk factors identify most fibril-forming kappa light chains. *Amyloid* **7**(3): 200–211.
Sunde M, Blake C. 1997. The structure of amyloid fibrils by electron microscopy and X-ray diffraction. *Adv. Protein Chem.* **50**: 123–159.
Takano K, Funahashi J, Yutani K. 2001. The stability and folding process of amyloidogenic mutant human lysozymes. *Eur. J. Biochem.* **268**(1): 155–159.
Tan SY, Pepys MB, Hawkins PN. 1995. Treatment of amyloidosis. *Am. J. Kidney Dis.* **26**(2): 267–285.
Thual C, Bousset L, Komar AA, Walter S, Buchner J, Cullin C, Melki R. 2001. Stability, folding, dimerization, and assembly properties of the yeast prion Ure2p. *Biochemistry* **40**(6): 1764–1773.
Wall J, Schell M, Murphy C, Hrncic R, Stevens FJ, Solomon A. 1999. Thermodynamic instability of human lambda 6 light chains: correlation with fibrillogenicity. *Biochemistry* **38**(42): 14101–14108.
Westermark P, Benson MD, Buxbaum JN, Cohen AS, Frangione B, Ikeda S, Masters CL, Merlini G, Saraiva MJ, Sipe JD. 2002. Amyloid fibril protein nomenclature—2002. *Amyloid* **9**(3): 197–200.

